Inhibitor selectivity: profiling and prediction

Janssen, A.P.A.

I believe that scientific knowledge has fractal properties, that no matter how much we learn, whatever is left, however small it may seem, is just as infinitely complex as the whole was to start with.
Isaac Asimov

9 Summary and Future Prospects

General summary

The research presented in this thesis addressed one of the main challenges in modern drug development: selectivity. The whole area of *target-based* drug discovery is built on the notion that a certain protein target is a key regulator in a biological process. Although the use of this concept as the basis for drug discovery could be debated[1], the importance of chemical modulators capable of selectively altering the activity of the target protein is undisputed. The importance of selective inhibitors is especially great when they are used to prove the therapeutic value of a certain target. Generally, a therapeutic window needs to

be determined where the target protein is selectively modulated. At higher concentrations the effects of binding other targets could lead to side-effects and possible toxicity.

Because of the importance of selectivity, many techniques have been developed to assess the exact binding profiles of inhibitors, such as family-wide activity assays (e.g. for kinases and luciferases), and more specific assays like the 44-member CEREP-panel.[2] Other, more untargeted approaches have been developed, e.g. Cellular Thermal Shift Assay (CETSA) and a variety of uses of radiolabelled drug analogues. Another technique which has proven to be highly flexible and thus has found a large variety of applications in (early) drug discovery is activity-based protein profiling (ABPP). The concept of this technique was explained in **Chapter 1**. One field of research where ABPP has shown great use is that involving the endocannabinoid system (ECS), which is under active investigation for its role in anti-nociceptive and anti-inflammatory effects, amongst others.[3–6] This signalling system consists of two cannabinoid receptors (CB1 and CB2), and two main endogenous ligands: 2-arachidonoylglycerol (2-AG) and *N*-arachidonoylethanolamine (anandamide), and their biosynthetic and catabolic enzymes. 2-AG is the most abundant endocannabinoid and is mainly produced by diacylglycerol lipase (DAGL) α and β. The different roles of the two endocannabinoids and the specific functions of the two isoforms of DAGL are still poorly understood. This warrants the search for selective and *in vivo* active inhibitors to be able to study these processes in more detail.

Diacylglycerol lipase inhibitors: activity and specificity

Chapter 2 introduced the hit-to-lead optimization of a novel DAGL inhibitor scaffold: the 1,2,4-triazole-sulfonamides. This molecular series was found in a previously reported high-throughput screen.[7] In this Chapter the structure activity relations around the core scaffold were explored by screening 65 variants of the HTS-hit molecule. The potency for DAGL-α varied 400-fold from an IC_{50} of approximately 1 μM to 2.5 nM. By screening the library in mouse brain proteome using ABPP, the most selective inhibitor was identified and selected for further profiling. Compound **1** (Figure 9.1), a 2-benzylpiperidine substituted triazole urea, was active in mouse Neuro-2a cells. To test *in vivo* target engagement, compound **1** and an alkynylated analogue were administered intraperitoneal to mice. The serine hydrolase activities were analysed in the brain and spleen using gel-based ABPP after two hours. Both compounds passed the blood-brain barrier and potently engaged DAGL-α in the brain.

A single dose of 50 mg/kg was predominantly chosen to demonstrate target engagement *in vivo*. Due to the high dose, off-target activity was observed. A dose-response experiment is advised, which is ideally coupled to pharmacokinetic measurements, to determine the optimal dose of target engagement with minimal off-target activity. Considering the weak inhibition of DAGL-β in the spleen, it is possible that a dose can be selected where DAGL-α is selectively inhibited. This would enable for the first time detailed investigations of the separate DAGL isoforms by acute inhibition. In light of the similarities in the inhibition profile of **1** and DH376[5], pairing the inhibitors might lead to the identification of DAGL-β-specific effects in, for example, feeding behaviour.[8]

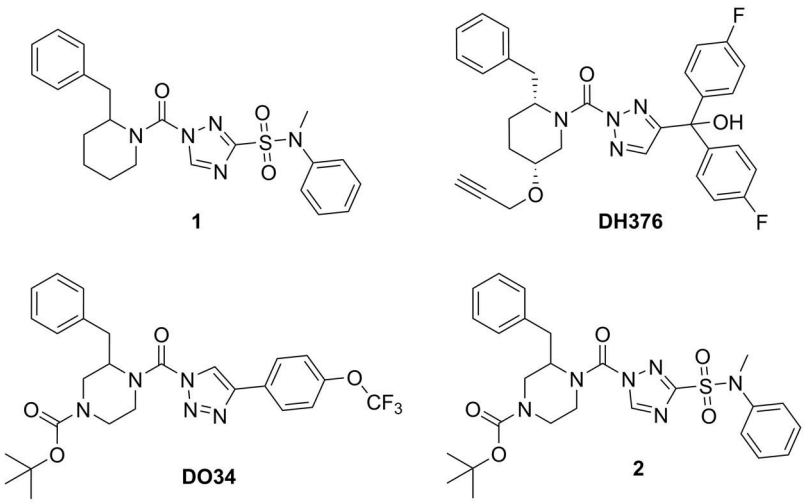

Figure 9.1 | Chemical structures of inhibitor **1**, reference inhibitors DH376 and DO34 and inhibitor **2**.

Chapter 3 was focussed on optimizing the physicochemical properties of compound **1**. In particular, the topological polar surface area (TPSA) was increased to restrict the inhibitors to the periphery to target predominantly DAGL-β. Hit optimization resulted in the discovery of highly potent compound **2**, in which the piperazine moiety of DO34 (Figure 9.1) was incorporated. Next, a small 24-membered library was synthesized in which the *tert*-butyl carbamate was replaced with various amides, ureas, tertiary amines and sulfonamides. This led to four highly potent and *in vitro* selective compounds, which were tested in Neuro-2a cells. A more than tenfold drop in IC_{50} values indicated that cell penetration was less efficient, possibly due to a reduced passive diffusion as a result of the increased polarity. Remarkably, the *in situ* the selectivity window was also reduced compared to the *in vitro* values.

Cellular profiling of the library is advised to assess potency and selectivity of different substitution patterns, ideally identifying more promising lead compounds. If more selective inhibitors are identified, an *in vivo* dose-response experiment should be performed to identify dosages that show full target engagement in peripheral tissue, but leave the brain unaffected. These compounds could then be instrumental in the elucidation of the workings and importance of the peripheral endocannabinoid signalling, and the role of DAGL-β in this process.

Chapter 4 showed the in depth investigation of the structure kinetic relationships of a small set of DH376 derivatives. A previously reported surrogate substrate assay was adapted to determine the affinity (K_i) and reactivity (k_{inact}) of mechanism-based covalent inhibitors.[3] DynaFit software[9] was used to fit a system of differential equations to the substrate conversion curves generated by this kinetics assay. Remarkably, the inactivation constants (k_{inact}) did not follow the trend in pK_a of the heterocycles, which is contradictory to standard theories of nucleofugality. In contrast, the change in number and position of the nitrogen atoms in the heterocycle strongly influenced the binding constant K_i. The 1,2,3-triazole based DH376 bound with picomolar affinity.

The approach to determine the binding affinity and reactivity presented in Chapter 4 is based on a traditional biochemical readout. Other novel techniques, such as Surface

Plasmon Resonance (SPR) and Isothermal Calorimetry (ITC), have recently been applied for in-depth evaluation of the formation of protein-inhibitor complexes.[10] The benefit of the here presented approach is its low cost and relatively high throughput: the current setup uses 96-well plates and allows for 6 compounds to be screened per (duplicate) plate and does not require purified enzymes. The original surrogate substrate assay was successfully miniaturized to 1536-well format, so there is room to improve the current throughput of the kinetics assay.[7] The assay could also be easily adopted by other enzymes capable of hydrolysing 4-nitrophenyl butyrate or alternative surrogate substrates. This could be especially relevant for major off-targets of the current series of inhibitors, like α/β-hydrolase domain containing protein 6 (ABHD6). This will guide the discovery of more selective DAGL inhibitors, including the inhibitors of Chapter 2 and 3.

Chapter 4 provided some key insights in the importance of the heterocycle of the DH376 variants to the binding affinity with DAGL-α. It should be investigated whether this SAR can be transferred to the triazole-sulfonamide series developed in Chapters 2 and 3. This can be achieved by synthesizing variants of **1** containing a 1,2,3-triazole (**3**) or pyrazole (**4**) (Scheme 9.1), in an analogous manner as presented in Chapters 2 and 3. Testing these compounds alongside **1** in the assay developed in Chapter 4 could provide novel insights in the binding-mode of these sulfonamide based inhibitors, and they may have interestingly different interaction profiles.

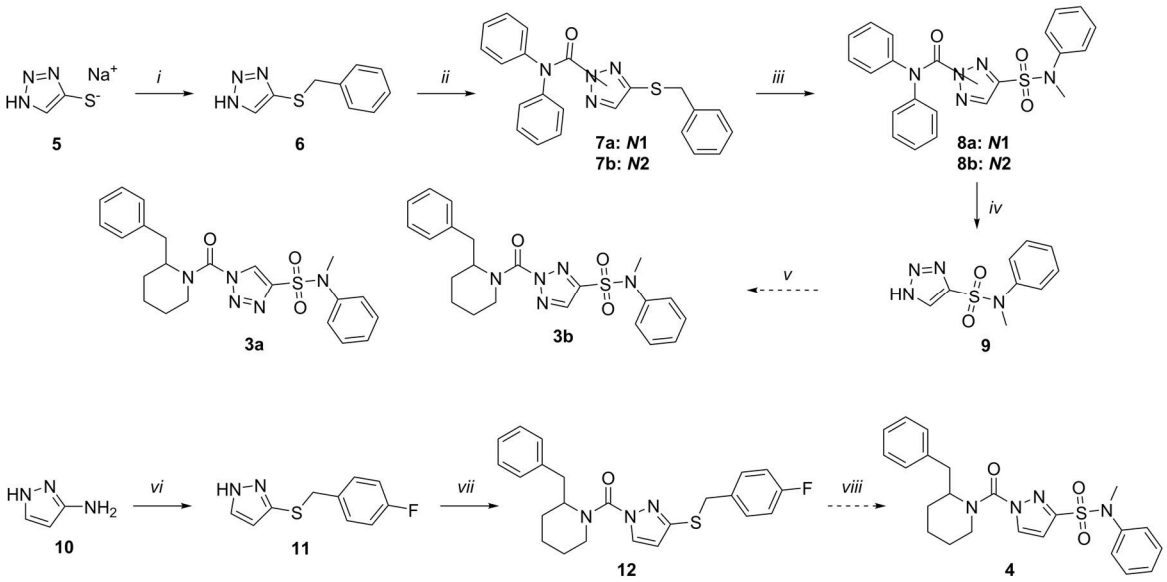

Scheme 9.1 | Synthesis of 1,2,3-triazoles (**3a** and **3b**) and pyrazole (**4**) derivatives of **1**. Reagents and conditions: *i*) benzylbromide, DMF, 18 h, 86%; *ii*) diphenylcarbamic chloride, DIPEA, DMAP, THF, 65 °C, 18 h, 71%; *iii*) HCl, NaOCl, DCM, -10 °C, 20 min, then *N*-methylaniline, -10 °C → RT, 2h, 65%; *iv*) KOH, H_2O/THF (1:1 v/v), 18 h, 57%; *v*) 2-benzylpiperidine, triphosgene, K_2CO_3, DCM, 0 °C → RT, 1 h, then **9**, DIPEA, THF, 6 h, 65 °C; *vi*) $NaNO_2$, H_2SO_4, H_2O, then NaOAc, NaOH, 4-fluorobenzylmercaptan, H_2O, 1 h, 0 °C, 42%; *vii*) 2-benzylpiperidine, triphosgene, DIPEA, THF, 0 °C, 1 h, then **11**, DIPEA, DMAP, THF, 65 °C, 6 h, 48%; *viii*) HCl, NaOCl, DCM, -10 °C, 20 min, then *N*-methylaniline, -10 °C → RT, 2h.

Activity-based protein profiling to study inhibitor selectivity

Chapter 5 showcased the utility of activity-based protein profiling in a highly relevant study to profile the interactions of the lethal drug-candidate BIA 10-2474, which was developed as a fatty acid amide hydrolase (FAAH) inhibitor. During the first-in-human phase 1 clinical trial held in France in early 2016, 5 members of the highest dosing group were hospitalised with severe neurological symptoms.[11] One of these volunteers succumbed to his symptoms several days after hospitalisation. The main hypothesis to explain the severe side effects was the possibility of off-target interactions. To investigate this, BIA 10-2474 was resynthesised, along with three alkyne-bearing analogues. The inhibitory capacity of BIA 10-2474 was assayed in a large panel of endocannabinoid related enzymes and both CB-receptors, and was found to only inhibit FAAH weakly *in vitro*. The interaction profile across nearly 50 serine hydrolases was assessed by ABPP using mouse brain proteomes. ABHD6 was found as an off-target at similar concentrations required for full FAAH inhibition. The covalent mechanism of action of the imidazole urea was shown by the fluorescent labeling of both FAAH and ABHD6 using 'Click'-chemistry on the alkyne analogues under denaturing SDS-PAGE conditions. *In situ* profiling of the inhibitors showed a large increase in potency for both FAAH and ABHD6, not observed for the safe FAAH inhibitor PF-04457845.[12] Using chemical proteomic profiling of *in situ* treated human neural cell cultures with BIA 10-2474 more off-targets were identified, which were subsequently verified by overexpression and competitive ABPP. Of note, these off-targets were not shared with PF-04457845, a safe FAAH inhibitor tested in phase 2 clinical trials, and were all involved in lipid metabolism. Finally, lipid analysis using targeted lipidomics showed a strong disruption of lipid networks in cultured neurons. This suggests that promiscuous lipase inhibitors have the potential to cause metabolic dysregulation in the nervous system. The importance of thorough off-target profiling, possible using ABPP, is emphasized and recommended.

None of the reported animal models used during pre-clinical characterization showed toxicity similar to that observed in humans.[13] Therefore, the assays performed here on mouse brain lysates and (neural) cell cultures should be repeated on actual patient-derived brain tissue samples. However, a call for access to the existing patient-material, such as blood samples from the trial, including those of unharmed volunteers, has not been followed up on by the sponsor of the trial, Bial Pharmaceuticals, thus making any further research in this direction infeasible.[14]

Another avenue of exploration could be the identification of protein interaction partners of BIA 10-2474 that were not targeted by activity-based probes used in the current study. To this end, chemical probes were generated based on the structure of BIA 10-2474, thereby creating an ABP closely related to the parent molecule. These probes, however, did not bind other targets than visualized in the competitive gel-based ABPP experiments with FP-TAMRA and MB064. The limitation of this approach is that the targets have to bind covalently to the urea electrophile to be visualized. Non-covalent interactions with proteins cannot be identified in this manner. Radioactively labelled BIA 10-2474 could aid in finding binding partners, but identification of specific proteins would be cumbersome. CETSA could be used, but will only reveal targets that are significantly thermally stabilized upon binding of BIA 10-2474. Photoaffinity labelling, combined with chemical biology methods, can be

used to identify non-covalent interaction partners.[15,16] This approach requires a photoreactive group to be present in the molecule. Typically, diazirines or benzophenones are used, but many other photoreactive groups exist.[15] An intriguing possibility arises in the case of BIA 10-2474, since the photoreactivity of heterocyclic *N*-oxides has been studied for decades for use in synthetic applications, but, to the best of my knowledge, has never been applied in a chemical biology setting.[17,18] Irradiation with ultraviolet light triggers a sequence of rearrangements, leading, in controlled conditions, to various reaction products.[17] No information is available regarding the reactivity of these species in close proximity to proteins. Experimental validation of this approach could consist of photolabelling experiments where the three alkynylated probes are irradiated. Incubation with or without BIA 10-2474 or the reduced pyridine metabolite BIA 10-2639, which should not be UV-active, can help to identify specific interactions. Conjugation to biotin using 'Click'-chemistry and consecutive enrichment for chemical proteomics should show the applicability of this photoreactive group in chemical biology. If successful, the abundance of pyridines and pyrimidines in drug-like molecules could open up a whole new field of target identification using heterocyclic *N*-oxides as photolabel. Finally, by applying computational target prediction algorithms on the BIA 10-2474 structure the amount of targets that need to be considered could be reduced, or at least the order of exploration could be optimized.

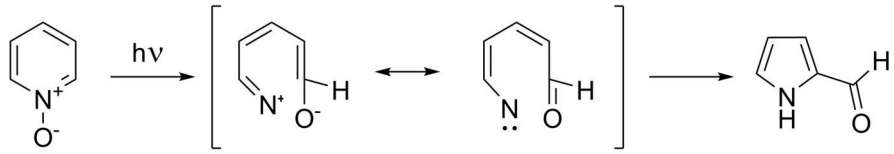

Scheme 9.2 | Proposed intermediates in the photoreaction of pyridine *N*-oxides.[17] The mechanism towards the bracketed transition state is not clear, and is believed to occur at a hyperplane.[18]

Chapter 6 described the development and in-depth characterisation of a green-fluorescent fluorophosphonate-probe, BODIPY-FP, an analogue of the widely used red-fluorescent TAMRA-fluorophosphonate. This new probe can be used in conjunction with the tailored DAG-lipase probe MB064, which carries a red-fluorescent BODIPY-TMR as reporter tag. The labeling efficiency of various enzymes with the new BODIPY-FP was found to be significantly different from TAMRA-FP. Especially the potency for FAAH and monoacylglycerol lipase (MAGL) was strongly increased. The probe was mixed at low concentration (10 nM) with MB064, thereby reliably visualising FAAH and MAGL without interfering with the labeling of MB064-targets. This probe cocktail allowed visualisation of most endocannabinoid related serine hydrolases in a single sample. This multiplex ABPP method was used to profile the selectivity of two MAGL inhibitors, NF1819 and ABX-1431.[19,20] The former was found to have several off-targets, including ABHD6. ABX-1431 showed no off-target activity up to 10 μM in mouse brain membrane proteome.

The combination of multiple probes with different reactive groups, also known as warheads, and orthogonal reporter tags, allows profiling of more proteins in a single sample. Especially in gel-based techniques broad reactivity of an ABP may lead to

overlapping protein bands, which hinders the quantification and identification. Since MB064 and BODIPY- or TAMRA-FP combined are not able to provide full coverage of the serine hydrolase family, the search for new activity-based probes is warranted. An interesting reactive group which has long been used in lipase inhibitors is the bromoenol lactone (BEL).[21] Previously, the introduction of a ligation handle in the form of an alkyne was proposed, but the synthesis proved cumbersome.[22] An alternative approach was envisioned based on a published synthetic procedure towards guanidine-containing protease inhibitors (Scheme 9.3).[23] This synthetic route furbished BEL probe **13** and a closely related inhibitor **14**.

Initial experiments using probe **13** *in situ* in a panel of breast cancer cell lines indicated that the BEL warhead is indeed able to covalently label several proteins in these cells in a dose-dependent manner (Figure 9.2). Most but not all bands could be outcompeted with pre-incubation of **14**, indicating specific targeting of several proteins. Chemical proteomics is required to identify the probe-targets, and to compare its interaction profile with fluorophosphonate-based probes.

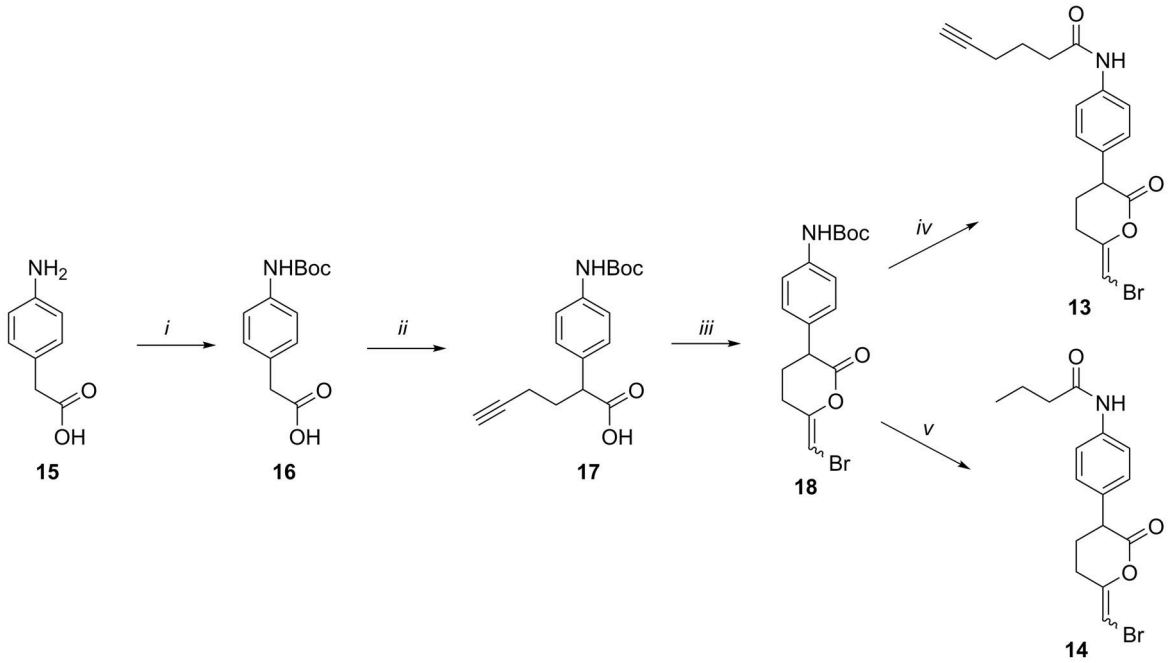

Scheme 9.3 | Synthesis of bromoenol lactone probe **13** and closely related inhibitor **14**. Reagents and conditions: *i*) Boc_2O, DCM, 18 h, 77%; *ii*) BuLi, THF, -30 °C, 30 min, then 4-bromobut-1-yne, -20 °C → 0 °C, 3 h, 40%; *iii*) K_2CO_3, DCM, then NBS, H_2O, 5 h, 22%; *iv*) TFA, DCM, 0 °C → RT, 1.5 h, then hex-6-ynoyl chloride, TEA, 0 °C 2 h, 53%; *v*) TFA, DCM, 0 °C → RT, 1.5 h, then butyryl chloride, TEA, 0 °C, 2 h, 63%.

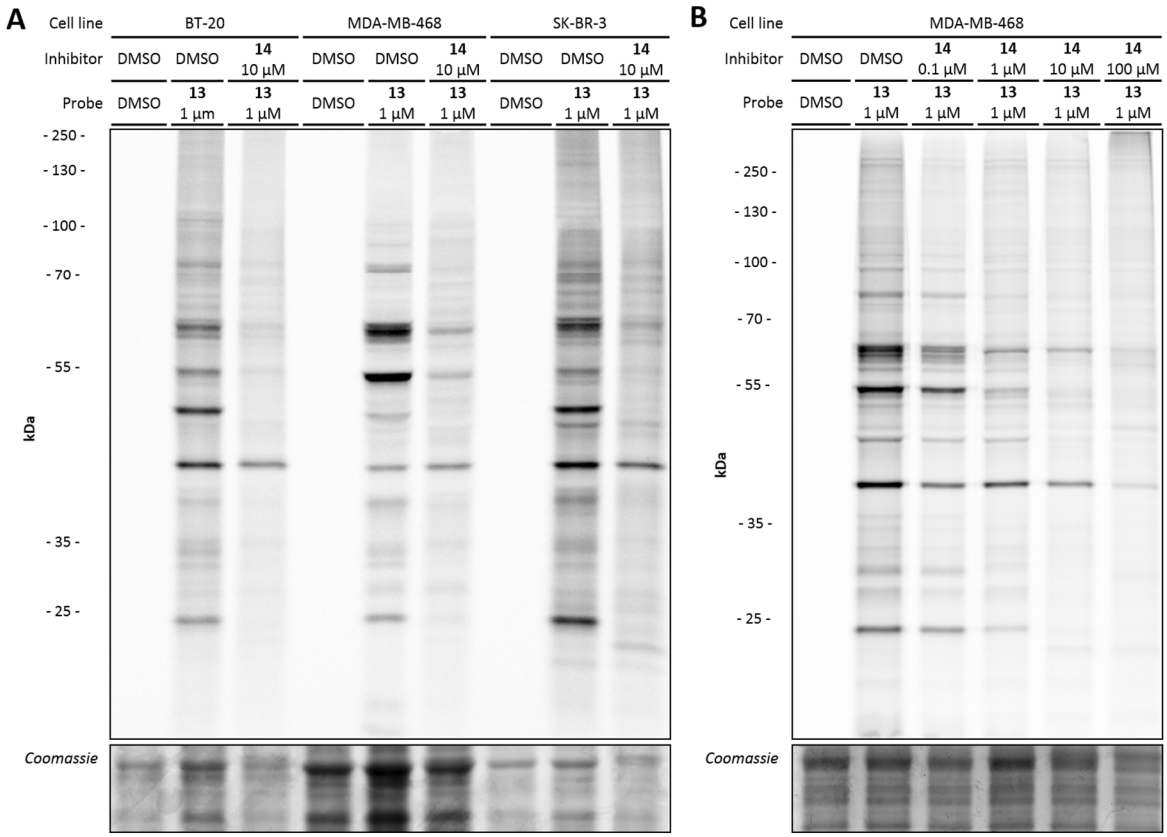

Figure 9.2 | Two-step labelling of breast cancer cell lines with BEL probe **13**, competed with a single dose (A) or a dose escalation (B) of inhibitor **14**. Coomassie staining is shown as protein loading control.

Machine learning as a tool to predict inhibition profiles

Chapter 7 introduced the application of the machine learning algorithm t-Distributed Stochastic Neighbour Embedding (t-SNE) as a similarity metric for (bio)molecules. In contrast to the commonly used Tanimoto coefficient (Tc), a bit string compatible distance metric, t-SNE generates a two dimensional visualisation of the high-dimensional bit string space, to some extent analogous to principal component analysis, which was shown to be outperformed by t-SNE in this context. t-SNE allows for a visual inspection of similar chemical matter, which is impossible when using the Tc. This similarity visualisation was applied to 2774 clinically used molecules as a demonstration of drug-like chemical space. This embedding showed strong co-localisation of chemically related compounds. t-SNE was further applied to a physicochemical bit string based on the alignment of the proteins of the serine hydrolase family. This revealed that t-SNE is capable of recapitulating phylogenetic information. The mapping of target-space was annotated with the inhibitory potencies of a diverse set of compounds, previously measured in an ABPP-based assay.[24] Despite the small datasets available for serine hydrolases, co-localisation of potently inhibited proteins could be observed, suggesting that this approach could be extended to predict affinities of inhibitors across an entire protein family.

Chapter 8 built upon the principles introduced in Chapter 7, but focussed on the large protein family of kinases. Very large screening sets are available for kinases, which facilitates machine learning approaches such as that described in Chapter 7. The protein

kinase space could be reliably mapped using t-SNE. This resulted in a very strong similarity between the previously published Kinase Family Tree[25] and the t-SNE map. The molecules of the Published Kinase Inhibitor Set, combined with the biological data available for ~200 kinases, provided a large training set to be used in the here developed model, which was named Drug Discovery Maps (DDM).[26,27] This model was validated using the data from Karaman *et al*. and shown to equal or outperform the state-of-the-art computational techniques, such as quantitative structure activity relations (QSAR) and proteochemometric modelling.[28,29] DDM was applied in a virtual high-throughput assay in search for new FMS-like tyrosine kinase 3 (FLT3) inhibitors. A positive predictive value of 41% was achieved, identifying 18 actives out of a predicted 44. Two of these hits were resynthesised and tested in MV4:11 cells. Both compounds were cellular active and the best compound showed single-digit nanomolar potency. The predicted off-targets were validated and around 70% of the predicted targets were found to be inhibited. The model was also used to predict the interaction profile of a commercially available set of compounds with a hinge-binding motif. 20 molecules were purchased and tested for their predicted activities against HIPK3 and PAK2. Unfortunately, no actives were identified amongst the purchased compounds, possibly due to a low coverage of the training data around these targets, or poor similarity between the molecules in the training set and the commercial library.

The workflow presented in Chapter 8 is flexible regarding the training data that is used in the t-SNE algorithm. Since the model is in essence retrained for every run, simply loading a different list of molecules with associated biological data will provide a new predictive model, which can then be optimised by tuning the hyperparameters. Implementing a larger training set, such as that described recently by Bembenek *et al.* could strongly improve the predictive capacities of the model, although perhaps hierarchical SNE should be used to avoid excessive computational times.[30,31] Alternatively, a completely different set of molecular data could be used, such as a binding dataset for the GPCRs, or different processes altogether, e.g. metabolic data, lipophilicity data or (cyto-)toxicity.

An interesting but challenging possibility of further exploration is the application of the concept of cross-modal, also known as multimodal, clustering.[32] This autonomous classification technique was designed to use two or more unrelated sensory inputs from the same observation, which can be interpreted in the broadest manner, to classify unannotated data points into an *a priori* unknown number of clusters. Cross-modal coupling could thus, theoretically, be implemented to use two or more t-SNE embeddings of the same set of entities but with different modalities. One set of modalities could be different settings in the t-SNE perplexity, which should translate to embeddings using a different 'resolution', shifting the focus of the embedding from more high-level structure (high perplexity) to subtler local differences (low perplexity), and combining those views in order to gain insight in similarities not immediately evident from either setting separately. Another promising direction would be to use the clustering of inhibitors based on (normalized) biological data in one embedding, and on a chemical fingerprint in another. Different molecular clusters, possibly far separated in chemical space, might show similar trends in inhibition profile. These effects could be picked up by cross-modal clustering, and could give a whole new aspect to the use of t-SNE embeddings in drug discovery.

Closing remarks

Less than 1 in 10 drug candidates that enter phase 1 clinical trials actually gets approved for human use. The high failure rate is in part due to unforeseen side effects or toxicity. A better understanding of the role of selectivity and a better insight in the off-target activities of drug candidates could greatly aid in preventing candidates to fail for these reasons. This thesis has tried to address some aspects in this challenging part of drug discovery. The use of activity-based protein profiling as presented in Chapters 2 and 3 in drug discovery and hit-to-lead optimization, and in Chapter 5 and 6 for the interaction profiling of a drug candidate, highlights the versatility and importance of this chemical biology technique. Combined with knowledge derived from biochemical assays, such as that developed in Chapter 4, ABPP can greatly aid the medicinal chemist. The recent surge in popularity of machine learning algorithms, backed by exponential growth of the amount of biological data available, holds great promise for drug discovery. Chapters 7 and 8 showed the applicability of one such algorithm, which was able to quite reliably predict interaction profiles. The challenges in finding, determining and predicting selectivity are far from solved, but, by incrementally expanding our understanding of the binding of small molecules to their (off-)targets, truly selective inhibitors might at some point become a reality or their necessity might be mitigated.

Acknowledgements

Sebastiaan Koenders and Else Botter are kindly acknowledged for the experimental validation of probe **13** and inhibitor **14**.

Methods

Chemical Biology Methods

Cell Culture

BT-20, MDA-MB-468 or SK-BR-3 cells were cultured at 37 °C under 5% CO_2 in RPMI medium containing 10% (v/v) Fetal Calf Serum (Thermo Fisher), penicillin and streptomycin (200 µg/mL each; Duchefa). Medium was refreshed every 2-3 days and cells were passaged twice a week at 80-90% confluence by trypsinisation and resuspension in fresh medium.
Cells lines were purchased from ATCC and were regularly tested for mycoplasma contamination. Cultures were discarded after 2-3 months of use.

In situ treatment of breast cancer cell lines

BT-20, MDA-MB-468 or SK-BR-3 cells were seeded in 6-well plates. *In situ* treatment was initiated 72 h later. Medium was aspirated and medium with serum containing inhibitor or DMSO as vehicle was added (0.1 % DMSO). After 1 h exposure to treatment medium at 37 °C, probe or DMSO as vehicle was added and incubated for 1 h at 37 °C. The medium was aspirated and cells were harvested, washed with PBS and flash frozen in liquid nitrogen and stored at -80 °C until further use.

Cell lysate preparation

Cell pellets were thawed on ice, resuspended in cold lysis buffer (2.5 U/mL benzonase and 1x protease inhibitor (Amresco) in Milli-Q water) and incubated on ice (15-30 min). Protein concentrations were determined by a Quick Start™ Bradford Protein Assay. The cell lysate was diluted to 1.0 mg/mL concentration in lysis buffer and diluted samples were flash frozen in liquid nitrogen and stored at -80 °C until further use.

Fluorescent ligation and gel-based analysis

The two-step labeling protocol was adapted from previously developed methods.[33] Click reagent was freshly prepared by mixing copper sulfate (25 µL, 18 mM in water), THPTA (5 µL, 18 mM in water), sodium ascorbate (15 µL, 150 mM in water), and AF-647 (5 µL, 90 µM in DMSO). Click reagent (5.0 µL) was added to each proteome (40 µL per condition), mixed by brief vortexing and incubated under continuous shaking (1 h, 37 °C). 15 µL of 4* Laemmli buffer was added. Samples were boiled (95 °C, 5 min) and 8 µg proteome per reaction (12 µL) was resolved on a 10% acrylamide SDS-PAGE gel (180 V, 75 min). Gels were scanned using Cy3 and Cy5 multichannel settings (605/50 and 695/55, filters respectively) and stained with Coomassie after scanning. Coomassie staining was performed as a protein loading control.

Synthetic Methods

General remarks

All reactions were performed using oven- or flame-dried glassware and dry solvents. Reagents were purchased from Alfa Aesar, Sigma-Aldrich, Acros, and Merck and used without further purification unless noted otherwise. All moisture sensitive reactions were performed under an argon or nitrogen atmosphere. ^{1}H and ^{13}C NMR spectra were recorded on a Bruker AV-300 (300 MHz), AV-400 (400 MHz) or DRX-500 (500 MHz). Used software for interpretation of NMR-data was Bruker TopSpin 1.3 and MestreNova 11.0. Chemical shift values are reported in ppm with tetramethylsilane or solvent resonance as the internal standard ($CDCl_3$: δ 7.26 for ^{1}H, δ 77.16 for ^{13}C; MeOD: δ 3.31 for ^{1}H, δ 49.00 for ^{13}C).[34] Data are reported as follows: chemical shifts (δ), multiplicity (s = singlet, d = doublet, dd = double doublet, td = triple doublet, t = triplet, q = quartet, quintet = quint, bs = broad singlet, m = multiplet), coupling constants *J* (Hz), and integration.
Liquid chromatography analysis was performed on a Finnigan Surveyor LC/MS system, equipped with a C18 column. Flash chromatography was performed using SiliCycle silica gel type SiliaFlash P60 (230−400 mesh). TLC analysis was performed on Merck silica gel 60/Kieselguhr F254, 0.25 mm. Compounds were visualized using $KMnO_4$ stain (K_2CO_3 (40 g), $KMnO_4$ (6 g), and water (600 mL)) or CAM stain ($Ce(NH_4)_4(SO_4)_4{\cdot}2H_2O$ (ceric ammonium sulfate: 10 g); ammonium molybdate (25 g); conc. H_2SO_4 (100 mL); H_2O (900 mL)). Preparative HPLC (Waters, 515 HPLC pump M; Waters, 515 HPLC pump L; Waters, 2767 sample manager; Waters SFO System Fluidics Organizer; Waters Acquity Ultra Performance LC, SQ Detector; Waters Binary Gradient Module) was performed on a Waters XBridgeTM column (5 µM C18, 150 x 19 mm). Diode detection was done between 210 and 600 nm. Gradient: ACN in (H_2O + 0.2% TFA). High resolution mass spectra (HRMS) were recorded by direct injection on a q-TOF mass spectrometer (Synapt G2-Si) equipped with an electrospray ion source in

positive mode with Leu-enkephalin (m/z = 556.2771) as an internal lock mass. The instrument was calibrated prior to measurement using the MS/MS spectrum of Glu-1-fibrinopeptide B.

4-(Benzylthio)-1*H*-1,2,3-triazole (**6**)

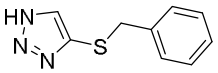

Sodium 1*H*-1,2,3-triazole-4-thiolate (1.23 g, 10.0 mmol) was dissolved in DMF (25 mL) and benzyl bromide (1.31 mL, 11.0 mmol) was added. The mixture was stirred for 18 h. The volatiles were removed under reduced pressure. The residue was purified by column chromatography to yield the title compound as an off-white solid (1.65 g, 8.64 mmol, 86%). ^{1}H NMR (300 MHz, $CDCl_3$) δ 14.54 (s, 1H), 7.48 (s, 1H), 7.21 – 7.05 (m, 5H), 4.04 (s, 2H). ^{13}C NMR (75 MHz, $CDCl_3$) δ 138.32, 137.00, 131.99, 128.73, 128.38, 127.26, 39.51.

4-(Benzylthio)-*N,N*-diphenyl-1,2,3-triazole-carboxamide (**7**)

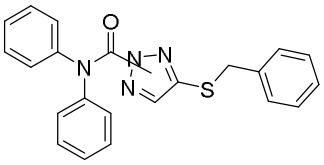

6 (1.248 g, 6.53 mmol) was dissolved in dry THF (30 mL) and diphenylcarbamic chloride (1.66 g, 7.18 mmol), DIPEA (1.37 mL, 7.83 mmol) and a catalytic amount of DMAP were added. The mixture was refluxed for 18 h. The reaction was quenched by the addition of sat. aq. Na_2CO_3 (40 mL). The organic layer was separated and the aqueous phase extracted with EtOAc (2x 40 mL). The combined organic layers were washed with brine (40 mL), dried ($MgSO_4$), filtered and concentrated. Column chromatography afforded the title compound as an off-white solid, consisting of a mixture of 2 regioisomers (2:1) (1.79 g, 4.62 mmol, 71%). Regioisomer 1: ^{1}H NMR (400 MHz, $CDCl_3$) δ 7.47 – 6.60 (m, 16H), 3.84 (s, 2H). Regioisomer 2: ^{1}H NMR (400 MHz, $CDCl_3$) δ 7.47 – 6.59 (m, 16H), 3.69 (s, 2H) (spectrum shows a mixture of rotamers). ^{13}C NMR (101 MHz, $CDCl_3$) δ 151.18, 141.32, 137.43, 136.75, 133.21, 130.15, 129.68, 129.55, 129.00, 128.66, 128.57, 128.50, 127.32, 127.24, 127.21, 127.18, 126.95, 107.18, 106.05, 39.01, 37.26.

4-(*N*-Methyl-*N*-phenylsulfamoyl)-*N,N*-diphenyl-1,2,3-triazole-carboxamide (**8**)

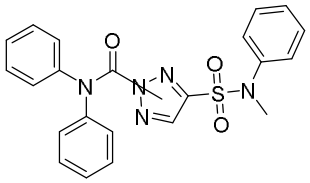

4 N HCl in dioxane (5 mL) was added to DCM (20 mL) and cooled to -10 °C. 15%$_{wt}$ NaOCl (aq., 5 mL) was added slowly, forming a yellow-green Cl_2 solution. After 30 min **7** (500 mg, 0.259 mmol) was added dropwise as a solution in DCM (5 mL). After 20 min *N*-methylaniline (5.0 mL, 46 mmol) was added. The mixture was stirred for 2 h at RT. The reaction was quenched by the addition of 0.1 M HCl (20 mL). The organic layer was separated and the water layer was extracted with EtOAc (2x 20 mL). The combined organic layers were dried ($MgSO_4$), filtered and concentrated. The residue was purified by column chromatography to yield the title compound as a brown solid (364 mg, 0.840 mmol, 65%). ^{1}H NMR (400 MHz, $CDCl_3$) δ 7.58 (s, 1H), 7.45 – 6.79 (m, 15H), 3.01 (s, 3H). ^{13}C NMR (101 MHz, $CDCl_3$) δ 147.92, 146.72, 141.68, 140.04, 136.10, 129.50, 129.05, 127.98, 127.61, 126.70, 126.28, 38.67.

N-Methyl-*N*-phenyl-1*H*-1,2,3-triazole-4-sulfonamide (**9**)

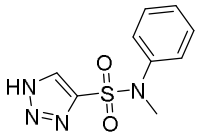

8 (364 g, 0.84 mmol) was dissolved in 1 N KOH in a 1:1 (v/v) H_2O/THF mixture (20 mL). The mixture was stirred for 18 h at RT. The mixture was concentrated and the residue was purified by column chromatography to yield the title compound (114 mg, 0.48 mmol, 57%). ^{1}H NMR (400 MHz, MeOD) δ 8.06 (s, 1H), 7.35 – 7.09 (m, 5H), 3.32 (s, 3H). ^{13}C NMR (101 MHz, MeOD) δ 145.60, 142.37, 130.68, 130.07, 128.78, 127.98, 39.25.

3-((4-Fluorobenzyl)thio)-1*H*-pyrazole (**11**)

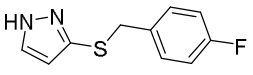

1*H*-Pyrazol-3-amine **10** (100 mg, 1.20 mmol) was dissolved in 40% aq. H_2SO_4 (5 mL). Sodium nitrite (100 mg, 1.44 mmol) in water (5 mL) was added slowly, keeping the temperature below 5 °C. After 15 minutes saturated aqueous NaOAc was added until the pH was ~5. The mixture was then added slowly to a cooled (0 °C) solution of (4-fluorophenyl)methanethiol (118 µL, 137 mg, 0.963 mmol) in 1 N aqueous NaOH (1 mL). A precipitate formed immediately upon addition. After addition was complete, the mixture was stirred for 1 h at 0 °C. The reaction mixture was extracted with EtOAc (3x 20 mL). The combined organic layers were washed with brine, dried ($MgSO_4$), filtered and concentrated. Column chromatography yielded the title compound (105.7 mg, 0.508 mmol, 42%) as a white solid. ^{1}H NMR (400 MHz, MeOD) δ 7.54 (d, *J* = 2.2 Hz, 1H), 7.25 – 7.15 (m, 2H), 6.97

– 6.89 (m, 2H), 6.20 (d, *J* = 2.2 Hz, 1H), 4.02 (s, 2H). ^{13}C NMR (101 MHz, MeOD) δ 163.31 (d, *J* = 244.1 Hz), 135.44, 131.65 (d, *J* = 8.1 Hz), 115.94 (d, *J* = 21.7 Hz), 109.97, 39.60.

(2-Benzylpiperidin-1-yl)(3-((4-fluorobenzyl)thio)-1*H*-pyrazol-1-yl)methanone (**12**)

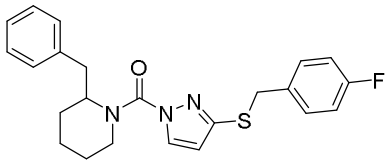

2-Benzylpiperidine hydrochloride (50.8 mg, 0.240 mmol) and triphosgene (71.2 mg, 0.240 mmol) were dissolved in dry THF (10 mL) at 0 °C. DIPEA (194 µL, 1.2 mmol) was added and the resulting mixture was stirred for 1 h. The mixture was poured into ice water (10 mL) and the organic layer was separated. The aqueous layer was extracted with EtOAc (3x 10 mL). The combined organic layers were dried ($MgSO_4$), filtered and concentrated under reduced pressure. The residue was taken up in dry THF (10 mL) to which **11** (50 mg, 0.24 mmol), DMAP (29.3 mg, 0.24 mmol) and DIPEA (194 µL, 1.2 mmol) were added. The mixture was heated to reflux for 6 h, after which it was poured into a saturated aqueous NH_4Cl solution (10 mL). The organic layer was separated and the aqueous layer was extracted with EtOAc (2x 10 mL). The combined organic layers were dried ($MgSO_4$), filtered and concentrated. Column chromatography afforded the title compound (47.3 mg, 0.116 mmol, 48%) as a white solid. ^{1}H NMR (400 MHz, $CDCl_3$) δ 7.64 (s, 1H), 7.38 – 6.89 (m, 9H), 6.11 (d, *J* = 2.8 Hz, 1H), 4.87 (s, 1H), 4.33 – 4.25 (m, 1H), 4.21 (t, *J* = 12.8 Hz, 2H), 3.28 – 2.97 (m, 2H), 2.84 (t, *J* = 10.7 Hz, 1H), 1.88 – 1.53 (m, 6H).

2-(4-((*tert*-Butoxycarbonyl)amino)phenyl)acetic acid (**16**)

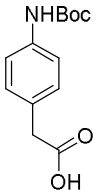

2-(4-Aminophenyl)acetic acid **15** (1.0 g, 6.62 mmol) was dissolved in DCM (20 mL). Boc-anhydride (1.54 mL, 6.62 mmol) was added and the mixture was stirred for 18 h at RT. The mixture was concentrated under reduced pressure. The residue was purified by column chromatography. The title compound was obtained as an orange solid (1.28 g, 5.09 mmol, 77%). ^{1}H NMR (400 MHz, MeOD) δ 8.75 (s, 1H), 7.34 (d, *J* = 8.2 Hz, 2H), 7.20 – 7.11 (m, 2H), 3.52 (s, 2H), 1.50 (s, 9H). ^{13}C NMR (101 MHz, MeOD) δ 175.67, 155.16, 139.14, 129.89, 119.81, 80.70, 41.18, 28.69.

2-(4-((*tert*-Butoxycarbonyl)amino)phenyl)hex-5-ynoic acid (**17**)

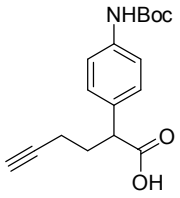

16 (620 mg, 2.47 mmol) was dissolved in THF (25 mL) and cooled to -30 °C, butyllithium (1.6 M in pentane, 5.09 mL, 8.14 mmol) was added dropwise. The mixture was stirred for 30 min. 4-Bromobut-1-yne (0.764 mL, 8.14 mmol) was slowly added and the mixture stirred for 2 h at -20 °C. The mixture was left to warm up to 0 °C over the course of 1 h. The reaction was quenched by the addition of ice. The organic layer was separated. The waterlayer was acidified to pH ~ 2 with 2 N HCl (aq.) and extracted with EtOAc (3x 50 mL). The combined organic layers were dried ($MgSO_4$), filtered and concentrated. The residue was purified using flash column chromatography. The desired product was obtained as a white powder (302 mg, 0.996 mmol, 40%). ^{1}H NMR (400 MHz, $CDCl_3$) δ 9.71 (bs, 1H), 7.41 – 7.06 (m, 4H), 6.74 (bs, 1H), 3.82 – 3.64 (m, 1H), 2.36 – 2.14 (m, 2H), 2.14 – 1.86 (m, 3H), 1.51 (s, 9H). ^{13}C NMR (101 MHz, $CDCl_3$) δ 179.44, 137.86, 132.24, 128.75, 119.26, 83.05, 69.62, 49.29, 31.36, 28.38, 16.28.

tert-Butyl (4-(6-(bromomethylene)-2-oxotetrahydro-2*H*-pyran-3-yl)phenyl)carbamate (**18**)

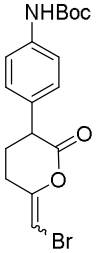

17 (150 mg, 0.494 mmol) was dissolved in dry DCM (7 mL). K_2CO_3 (41 mg, 0.30 mmol) was added to the solution. The resulting suspension was degassed for 15 min in a sonicator under continuous N_2-flow. *N*-Bromosuccinimide (97 mg, 0.54 mmol) and water (36 µL, 2 mmol) were added and the mixture was stirred for 5 h. The reaction mixture was quenched by the addition of $Na_2S_2O_3$ (5% aq., 10 mL). The organic layer was separated and diluted with DCM (10 mL), washed with H_2O (10 mL) and brine (5 mL). The combined organic layers were dried ($MgSO_4$), filtered and concentrated. The residue (yellow oil) was purified by column chromatography to yield the title compound as a white solid (42 mg, 0.11 mmol, 22%). ^{1}H NMR (400 MHz, $CDCl_3$) δ 7.44 – 7.30 (m, 2H), 7.18 – 7.07 (m, 2H), 6.60 (s, 1H), 6.12 – 6.03 (m, 1H), 3.74 (dd, *J* = 10.4, 5.4 Hz, 1H), 2.89 – 2.58 (m, 2H), 2.29 – 2.06 (m, 2H), 1.51 (s, 9H). ^{13}C NMR (101 MHz, $CDCl_3$) δ 168.76, 152.81, 151.62, 138.08, 131.42, 128.65, 118.98, 91.53, 80.79, 46.72, 28.42, 25.87, 23.84.

Hex-5-ynoyl chloride (**19**)

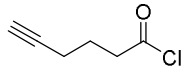

Hex-5-ynoic acid (0.197 mL, 1.78 mmol) was dissolved in DCM (10 mL) and oxalyl chloride (1.56 mL, 17.8 mmol) was slowly added. The mixture was refluxed for 2 h. The solvent and excess oxalyl chloride were removed *in vacuo* and the resulting oil was coevaporated twice with toluene. The crude hex-5-ynoyl chloride was used without further purification.

N-(4-(6-(bromomethylene)-2-oxotetrahydro-2*H*-pyran-3-yl)phenyl)hex-5-ynamide (**13**)

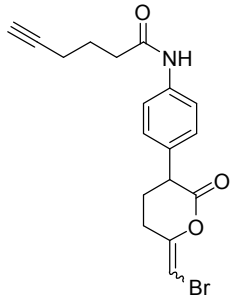

To a stirred solution of **18** (30 mg, 0.078 mmol) in DCM (3 mL) at 0 °C trifluoroacetic acid (0.302 mL, 3.92 mmol) was added. The mixture was stirred for 1.5 h at RT. **19** (102 mg, 0.785 mmol) was added and the mixture was cooled to 0 °C. TEA (0.60 mL, 4.3 mmol) was added and the mixture was stirred for 2 h at RT. The volatiles were evaporated under reduced pressure. Flash column chromatography yielded the title compound (15.6 mg, 0.041 mmol, 53%) as a white solid. ^{1}H NMR (400 MHz, $CDCl_3$) δ 7.58 – 7.45 (m, 2H), 7.40 (s, 1H), 7.21 – 7.11 (m, 2H), 6.11 (t, *J* = 1.8 Hz, 1H), 3.75 (dd, *J* = 10.6, 5.4 Hz, 1H), 2.96 – 2.81 (m, 1H), 2.76 – 2.64 (m, 1H), 2.51 (t, *J* = 7.3 Hz, 2H), 2.35 – 2.29 (m, 2H), 2.29 – 2.08 (m, 2H), 2.02 (t, *J* = 2.6 Hz, 1H), 1.94 (q, *J* = 7.3 Hz, 2H). ^{13}C NMR (101 MHz, $CDCl_3$) δ 170.74, 168.78, 151.55, 137.53, 132.76, 128.71, 120.31, 91.71, 83.55, 69.60, 46.88, 36.04, 25.89, 24.00, 23.94, 17.90. HRMS: Calculated for $[C_{18}H_{18}BrNO_3 + H]^+$ = 376.0542, found = 376.0548.

N-(4-(6-(Bromomethylene)-2-oxotetrahydro-2*H*-pyran-3-yl)phenyl)butyramide (**14**)

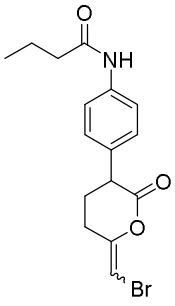

18 (10 mg, 0.026 mmol) was dissolved in DCM (1 mL) and trifluoroacetic acid (101 µL, 1.31 mmol) was added. The mixture was stirred for 1.5 h at RT, after which TLC showed full conversion of starting material. Butyryl chloride (27.1 µL, 0.262 mmol) was added and the mixture was cooled to 0 °C. Triethylamine (201 µL, 1.44 mmol) was added and the mixture stirred for 2 h at RT. The reaction mixture was concentrated and purified by column chromatography to yield the title compound (5.81 mg, 0.016 mmol, 63%) as a white solid. ^{1}H NMR (400 MHz, $CDCl_3$) δ 7.52 (d, *J* = 8.4 Hz, 2H), 7.21 – 7.11 (m, 3H), 6.11 (t, *J* = 1.8 Hz, 1H), 3.76 (dd, *J* = 10.5, 5.4 Hz, 1H), 2.93 – 2.81 (m, 1H), 2.77 – 2.63 (m, 1H), 2.34 (t, *J* = 7.4 Hz, 2H), 2.29 – 2.06 (m, 2H), 1.76 (h, *J* = 7.4 Hz, 2H), 1.01 (t, *J* = 7.4 Hz, 3H). ^{13}C NMR (101 MHz, $CDCl_3$) δ 168.69, 151.57, 137.63, 132.69, 128.74, 120.26, 91.69, 46.87, 39.81, 25.91, 23.92, 19.18, 13.88.

HRMS: Calculated for $[C_{16}H_{18}BrNO_3 + H]^+$ = 352.0542, found = 352.0544.

References

1. Croston, G. E. The utility of target-based discovery. *Expert Opin. Drug Discov.* **12**, 427–429 (2017).
2. Bowes, J. *et al.* Reducing safety-related drug attrition: the use of in vitro pharmacological profiling. *Nat. Rev. Drug Discov.* **11**, 909–922 (2012).
3. Baggelaar, M. P. *et al.* Development of an Activity-Based Probe and In Silico Design Reveal Highly Selective Inhibitors for Diacylglycerol Lipase-α in Brain. *Angew. Chemie Int. Ed.* **52**, 12081–12085 (2013).
4. Baggelaar, M. P. *et al.* Highly Selective, Reversible Inhibitor Identified by Comparative Chemoproteomics Modulates Diacylglycerol Lipase Activity in Neurons. *J. Am. Chem. Soc.* **137**, 8851–8857 (2015).
5. Ogasawara, D. *et al.* Rapid and profound rewiring of brain lipid signaling networks by acute diacylglycerol lipase inhibition. *Proc. Natl. Acad. Sci.* **113**, 26–33 (2016).
6. Baggelaar, M. P. *et al.* Chemical Proteomics Maps Brain Region Specific Activity of Endocannabinoid Hydrolases. *ACS Chem. Biol.* **12**, 852–861 (2017).
7. Janssen, F. J. Discovery of sulfonyl-1,2,4-triazole ureas as DAGLα inhibitors by HTS-ABPP. in *Discovery of novel inhibitors to investigate diacylglycerol lipases and α/β-hydrolase domain 16A* 109–139 (2016).
8. Deng, H. *et al.* Triazole Ureas Act as Diacylglycerol Lipase Inhibitors and Prevent Fasting-Induced Refeeding. *J. Med. Chem.* **60**, 428–440 (2017).
9. Kuzmič, P. DynaFit--a software package for enzymology. *Methods Enzymol.* **467**, 247–80 (2009).
10. Narayan, K. & Carroll, S. S. SPR Screening. in *Applied Biophysics for Drug Discovery* 93–105 (John Wiley & Sons, Ltd, 2017). doi:10.1002/9781119099512.ch6
11. Kerbrat, A. *et al.* Acute Neurologic Disorder from an Inhibitor of Fatty Acid Amide Hydrolase. *N. Engl. J. Med.* **375**, 1717–1725 (2016).
12. Johnson, D. S. *et al.* Discovery of PF-04457845: A Highly Potent, Orally Bioavailable, and Selective Urea FAAH Inhibitor. *ACS Med. Chem. Lett.* **2**, 91–96 (2011).
13. Bégaud, B. *et al.* Report by the Temporary Specialist Scientific Committee (TSSC), 'FAAH (Fatty Acid Amide Hydrolase)', on the causes of the accident during a Phase 1 clinical trial. 1–28 (2016).
14. Brøsen, K., Funck-Brentano, C., Kroemer, H. K., Pirmohamed, M. & Schwab, M. Open letter on access to the BIA 10-2474 clinical trial data. *Lancet* **375**, 1788–89 (2016).
15. Smith, E. & Collins, I. Photoaffinity labeling in target- and binding-site identification. *Future Med. Chem.* **7**, 159–183 (2015).
16. Soethoudt, M. *et al.* Selective Photoaffinity Probe That Enables Assessment of Cannabinoid CB 2 Receptor Expression and Ligand Engagement in Human Cells. *J. Am. Chem. Soc.* **140**, 6067–6075 (2018).
17. Lohse, C., Hagedorn, L., Albini, A. & Fasani, E. Photochemistry of pyridine-oxides. *Tetrahedron* **44**, 2591–2600 (1988).
18. Poole, J. S. Recent Advances in the Photochemistry of Heterocyclic N-Oxides and Their Derivatives. in *Heterocyclic N-Oxides* (ed. Oleg V. Larionov) 111–151 (Springer, 2017). doi:10.1007/7081_2017_4
19. Cisar, J. S. *et al.* Identification of ABX-1431, a Selective Inhibitor of Monoacylglycerol Lipase and Clinical Candidate for Treatment of Neurological Disorders. *J. Med. Chem.* **61**, 9062–9084 (2018).
20. Brindisi, M. *et al.* Development and Pharmacological Characterization of Selective Blockers of 2-Arachidonoyl Glycerol Degradation with Efficacy in Rodent Models of Multiple Sclerosis and Pain. *J. Med. Chem.* **59**, 2612–2632 (2016).
21. Daniels, S. B., Cooney, E., Sofia, M. J., Chakravarty, P. K. & Katzenellenbogen, J. A. Haloenol lactones. Potent enzyme-activated irreversible inhibitors for alpha-chymotrypsin. *J. Biol. Chem.* **258**, 15046–53 (1983).
22. Baggelaar, M. P. Summary and Future Prospects. in *Activity-based Protein Profiling of Diacylglycerol Lipases* 177–190 (2017).
23. Rai, R. & Katzenellenbogen, J. A. Guanidinophenyl-substituted enol lactones as selective, mechanism-based inhibitors of trypsin-like serine proteases. *J. Med. Chem.* **35**, 4150–9 (1992).
24. Bachovchin, D. A. *et al.* A high-throughput, multiplexed assay for superfamily-wide profiling of enzyme activity. *Nat. Chem. Biol.* **10**, 656–663 (2014).
25. Manning, G., Whyte, D. B., Martinez, R., Hunter, T. & Sudarsanam, S. The Protein Kinase Complement of the Human Genome. *Science* **298**, 1912–1934 (2002).
26. Drewry, D. H., Willson, T. M. & Zuercher, W. J. Seeding collaborations to advance kinase science with the GSK Published Kinase Inhibitor Set (PKIS). *Curr. Top. Med. Chem.* **14**, 340–2 (2014).
27. Elkins, J. M. *et al.* Comprehensive characterization of the Published Kinase Inhibitor Set. *Nat. Biotechnol.* **34**, 95–103 (2015).
28. Karaman, M. W. *et al.* A quantitative analysis of kinase inhibitor selectivity. *Nat. Biotechnol.* **26**, 127–132 (2008).
29. Christmann-Franck, S. *et al.* Unprecedently Large-Scale Kinase Inhibitor Set Enabling the Accurate Prediction of Compound–Kinase Activities: A Way toward Selective Promiscuity by Design? *J. Chem. Inf. Model.* **56**, 1654–1675 (2016).

30. Bembenek, S. D., Hirst, G. & Mirzadegan, T. Determination of a Focused Mini Kinase Panel for Early Identification of Selective Kinase Inhibitors. *J. Chem. Inf. Model.* **58**, 1434–1440 (2018).
31. Pezzotti, N., Höllt, T., Lelieveldt, B., Eisemann, E. & Vilanova, A. Hierarchical Stochastic Neighbor Embedding. *Comput. Graph. Forum* **35**, 21–30 (2016).
32. Coen, M. H. Cross-Modal Clustering. in *The Twentieth National Conference On Artificial Intelligence* 932–937 (2005).
33. Bachovchin, D. A. *et al.* Superfamily-wide portrait of serine hydrolase inhibition achieved by library-versus-library screening. *Proc. Natl. Acad. Sci.* **107**, 20941–20946 (2010).
34. Gottlieb, H. E., Kotlyar, V. & Nudelman, A. NMR Chemical Shifts of Common Laboratory Solvents as Trace Impurities. *J. Org. Chem.* **62**, 7512–7515 (1997).